**Journal of the Nigerian Society of Physical Sciences**

Original Research

# GPS-TEC Variations over the African Low-latitude Ionosphere during March 2013 and 2015 Geomagnetic Storms

S. O. Ikubanni[a,*], S. J. Adebiyi[a], B. O. Adebesin[a], O. S. Bolaji[b,c], B. J. Adekoya[d], B. W. Joshua[e], J. O. Adeniyi[a]

[a]*Space Weather Group, Landmark University, P.M.B. 1001, Omu-Aran, Nigeria*
[b]*Department of Physics, University of Lagos, Nigeria*
[c]*Department of Physics,University of Tansmania, Australia*
[d]*Department of Physics, Olabisi Onabanjo University, Ago-Iwoye, Ogun State*
[e]*Department of Physics, Kebbi State University, Aleiro, Kebbi State*

## Abstract

Intense geomagnetic storms offer opportunity to understand ionospheric response to space weather events. Using Total Electron Content (TEC) data from stations along the east African sector, the two most intense storms during the 24th solar cycle, with similarly occurrence season and time were studied. We observe that ionospheric effect during the main phase is not a function of the severity of the storm, whereas the more intense storm shows greater influence on the African ionosphere during the recovery phase. Plasma movement within the equatorial ionization anomaly (EIA) was evident particularly during the recovery phase, especially during the 2015 event. For both storms, the nighttime/early morning ionospheric effect is more pronounced than the daytime effects across all stations.

## 1. Introduction

Energetic mass particles released during solar storms impact the Earth's magnetosphere if earth-directed. This impact leads to perturbations in the various components of the Earth's magnetic field, in what is termed "geomagnetic storms" and subsequently causes rapid and sometimes substantial changes in ionospheric plasma distribution referred to as "ionospheric storms." Ionospheric response to magnetospheric perturbations depends on the driving conditions and ionospheric conductivity [1]. The disturbance of the Earth's magnetic field has varying severity, hence classified into categories. For classification of geomagnetic storms see [2]. There is a large body of literature documenting the ionospheric changes associated with the two recent St. Patrick Day geomagnetic storms of varying intensity, which occurred in March 2013 and 2015; periods around the solar maxima in solar cycle 24. Though, both storms can be classified as intense, the 2015 event was the first storm to make the severe category during the sunspot cycle 24 [3]. The two St. Patrick Day storms were triggered by Interplanetary Coronal Mass Ejection (ICME) but of different origins and with differ-

*Corresponding author tel. no: +2347032261146
Email address:* ikubanni.stephen@lmu.edu.ng (S. O. Ikubanni )

ent magnitudes [4]. A summary of some of the most recent and significant observations are presented in [5].

In this paper, we limit the review to published observations of ionospheric responses in the low latitude/equatorial regions. Hairston *et al.* [6] analysis of plasma flows, densities, composition, and temperatures obtained from five polar-orbiting Defence Meteoriological Satellite Program (DMSP) spacecraft operational during the storm and from the equatorial-orbiting Communications/Navigation Outage Forecasting system (C/NOFS) spacecraft revealed the influence of the prompt penetration electric field (PPEF) and the disturbance dynamo electric field (DDEF); as well as the resulting meridional (vertical) ion flows in the equatorial ionosphere during the March 2015 storm. The disturbed electric fields, which are the PPEF and DDEF, were decisive during both storms. During disturbed periods, errors in single-frequency Global Navigation Satellite Systems (GNSS) caused by ionospheric delays due to deviation from the quiet-time total electron content (TEC) average can be large, leading to loss of data, satellite signal degradation, breakdown in quality of communication links, reduced capacity for navigation and positioning [7].

The PPEF, which is usually short-lived, emerges due to the injection of electric field in the solar wind into the ionosphere, during the period of southward turning of the interplanetary magnetic field (IMF) [8] and it remarkably depends on local time [9]. For example, the PPEF caused a large increase in vertical plasma drift at local evening time, leading to equatorial spread-F irregularities/plasma bubbles and scintillation [10, 11]. IMF-Bz orientation during sunset can enhance or inhibit post sunset formation of equatorial irregularities; it inhibits if northward (as it occurred during the 2015 storm) and enhances if southward (as it occurred during the 2013 storm) [12]. Ray *et al.* [13] identified occurrence of equatorial spread-F (ESF) at the East Pacific and the Indian sectors due to the time of the southward turning of IMF-Bz.

The DDEF, usually long-lived, is a product of the enhanced energy injection into the auroral; which alters the global circulation and the generation of electric fields and currents [9]. The DDEF can cause generation of equatorial irregularities around sunrise, by causing large increase in the F2 peak height (hmF2) (as observed during both 2013 and 2015 storms in the 100 $^o E$ sector) [12]. Also, DDEFs exhibit remarkable local time dependence; due to the local time differences between different sectors as documented by [9], it caused intense negative ionospheric storm effects in the Asian-Australian equatorial sector and positive storm effects in the American equatorial sector during 2015 event. With analysis of data from both hemispheres, Kalita *et al.* [12] attributed the observed hemispherical asymmetry of electron density depletion to the asymmetric expansion of the storm-time thermospheric composition.

In another study, Nava *et al.* [13] noted that the largest storm effects occurred at longitudinal sectors that are on the evening/night sides during the time of very large energy inputs. In agreement, the disturbance dynamo was reported to have caused an upward ion drift (reaching 200 $ms^{-1}$) in the midnight-dawn sector, a downward ion drift (reaching 80 $ms^{-1}$) in the early morning sector and a westward ion drift (reaching around

100 $ms^{-1}$) near dawn [14]. Also, there was increase in the concentration of oxygen ion (O+) from < 60 % of the constituent ion before the storm to between 80 – 90 % during the 2015 storm; and attributed the sudden increase in O+ to the effect of disturbance neutral winds on the post-midnight equatorial ionosphere [14]. The disturbed neutral wind and the disturbed electric field could modify the equatorial ionization anomaly (EIA) in terms of the location and magnitude of the two crests with respect to quiet periods as seen in the 2013 storm [15]. Another study during the 2015 event[16] suggested the altitudinal dependence of the storm time electrodynamics of the topside ionosphere.

Observations of the geospace effects of the St. Patrick's Day storms over the African sector are very limited; some of the available ones include [17, 18, 19, 20]. Bolaji *et al.* [20] documented observations of equatorial ionospheric irregularities across several sectors, the African sector inclusive, using the Rate of Change of TEC index (ROTI) as indicator. Their work showed longitudinal variation in the strength of the irregularities partly due to the different local time effect of the storm-induced drivers. The irregularities decrease eastward from the American sector through the African sector, but not present in the Oceania. Also, the African equatorial/low-latitude ionosphere, during the 2015 event, experienced positive phases during the main phase and negative phases several hours after the storm commencement and during the recovery phase. The positive ionospheric storm during the MP was attributed to the PPEF while DDEF was suggestive of the negative phase and suppression of irregularities over all considered stations [19]. Amaechi *et al.*[19] report also showed that the northern EIA peak was formed beyond the 15$^o$ geographical latitude and the southern peak between the geographical equator and the −5$^o$ latitude. The limitation of [4], based on this, is that the southern stations employed all fall beyond the EIA crest. For this work, stations including those that fall within the 15 $^o N$ and 5 $^o S$ of the geographical equator have been employed. The stations were also chosen along close longitudes to reduce local time differences. Hence, the work is meant to contribute to the discourse on the geospace effects of the two recent St. Patrick's Day storms, using datasets from stations that have largely not been investigated for these storms.

## 2. Data and Methodology

We have employed data from the ACE satellite to describe the interplanetary solar wind characteristics that lead to the geomagnetic storms of 17 March 2013 and 17 March 2015. These data covers from the 16 – 20 March for both events and are provided by the National Space Science Data Centre (http://nssds cgsfc.nasa.gov/omniweb). These data include the Z-component of the Interplanetary Magnetic Field (IMF-Bz), which describes the orientation of the earth-directed Sun's magnetic field contained in the solar wind that impacts the Earth's magnetosphere, recorded in nanotesla (*nT*); the speed of the solar wind, recorded in kilometers per second (*km/s*); and the Interplanetary Electric Field (IEF) measured in millivolts per metre (*mV/m*). The other complementing information are geomagnetic parameters

obtained from ground-based observing instruments. These include the symmetric disturbance of the horizontal component of the Earth's magnetic field (SYM-H), which is the measure of perturbations in the H-component of the Earth's magnetic field due to the influence of ring currents and other current system in the magnetosphere [21]. SYM-H is a product of monitoring these perturbations at designated stations around the equatorial/low-latitude regions and recorded in nT; and Auroral Electrojet (AE) which is observed at designated stations in the polar/high-latitude region and recorded in nT.

Ionospheric electron density variation in the African low-latitude region was investigated using derived vertical Total Electron Content (vTEC)retrieved from raw observables from six (6) Global Positioning System (GPS) receivers. These work in particular focused on the symmetry of the northern and southern anomaly crests and the plasma reversal at the trough. Most of the observables in Receiver Independent Exchange (RINEX) format were retrieved from Scripps Orbit and Permanent Array Center (SOPAC) (ftp://garner.uscd.edu), while some (such as for Mtandika 'MTDK' and Solar village 'SOLA' stations) were retrieved from UNAVCO database (ftp://data-out.unavco.org/pub/rinex/obs/).Satellite and receiver biases contained in files from Center for Orbit Determination in Europe (CODE) and available at "ftp://ftp.unibe.ch/aiub/CODE" was also retrieved. TEC was obtained from the RINEX and CODE files by applying a procedure developed at the Boston College and package in the software "GPS v2.9.5", which is freely available at "http://seemala.blogspot.com/".Using some stations within the African EIA, we investigated the TEC magnitude at both crests of the EIA in relation to the trough, the asymmetry at the two crests and fountain plasma reversal during the storm main and recovery phases. The station names, their codes and geomagnetic coordinates are shown in Table 1. Figure 1 presents the position of these stations on the African map. For both storm events, five stations within the EIA were considered. One station is within the Equatorial Electrojet (EEJ) belt and the remaining four seasons fall equally on both sides of the magnetic equator, of the six stations listed in Table 1 only four (4) stations have for the 2013 and 2015 storm events considered. ZAMB has data for the period under consideration in 2013 while MTDK has data for 2015 only; hence, they were respectively adopted as the southern EIA crest station for the individual storm events. The deviation of storm-time electron density denoted as TEC was quantified as a percentage of the quiet-time reference. This is expressed as presented in equation 1.

$$\%\Delta TEC = \left( \frac{TEC_{disturbed} - TEC_{quiet}}{TEC_{quiet}} \right) \times 100\%, \qquad (1)$$

where $TEC_{disturbed}$ is the storm-time TEC values and $TEC_{quiet}$ is the quiet-time average TEC values. The quiet-time value is the mean from five most quiet days of the month. The selected quietest days were obtained from the German Research Centre for Geosciences (http://www.gfz-potsdam.de/en/section/earths-magnetic-field/data-products-services/kp-index/qd-days/qd-days-since-2010/). The values obtained from employing Equation 1 indicates either storm-induced changes when |%ΔTEC|

exceeds ±25% for at least 3 consecutive hours. Positive values indicate enhancements while negative values indicate depletions.
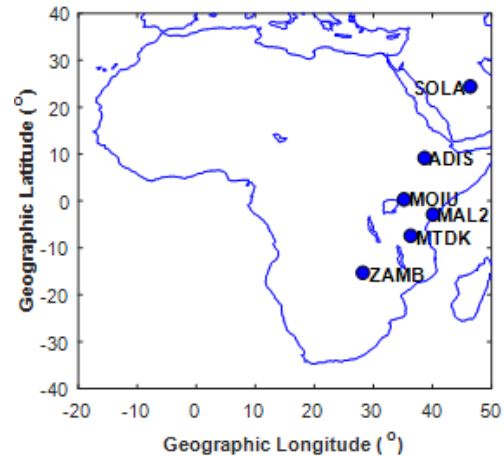


Figure 1. Map of Africa showing the stations used for this work.

## 3. Results and Discussion

### 3.1. Description of the storms

From the left panel of Figure 2, the 2013 storm-time interplanetary and geomagnetic parameters show a sharp southward turning of IMF-Bz to a magnitude of 14 *nT* around 0900 UT on 17 March (marking the beginning of the geo-effectiveness of the storm) shortly after the shock (sudden positive increase in SYM-H). The magnitude of IMF-Bz in the southward orientation decreases to about zero after 5 *hours*. It then increases to another peak (∼ 12 *nT*) at 1800 UT before gradually decreasing and then turning northward around 2300 UT. The shock occurred around 0600 UT on 17 March and produced a SYM-H value of ∼ 20 *nT*. The continuous injection of energy into the magnetosphere after the shock led to increase in the ring current and causing a depression in the SYM-H to a minimum of −132 *nT* around 2000 UT on 17 March. The interplanetary electric field, *E* increases abruptly from around zero at 0700 UT on 17 March to a peak of ∼ 10 *mV/m* three hours later. The magnitude of *E* then fluctuates as it decreases reaching approximately zero value at 1400 UT before increasing to another peak of ∼ 7 *mV/m* at 1800 UT on 17 March. The AE-index increased to 781 *nT* coinciding with the time of the shock and reached a peak of 1060 *nT* an hour later; it then decreases and fluctuates before increasing to another peak of ∼ 1800 *nT* around 1600 UT on 17 March. AE-index remained relatively high for another 7 *hours* (i.e. until around 2300 UT).

From the right panel of Figure 2, the 2015 storm-time interplanetary and geomagnetic parameters show a sharp increase in the IMF-Bz magnitude (∼ 20 *nT*) in the northward direction at 0500 UT on 17 March shortly after the shock arrival; and then instantly turned southward. The southward IMF-Bz reached a peak (∼ 16 *nT*) at 0800 UT (marking the beginning of the

Table 1. GPS stations, countries, and codes as well as their geographical and geomagnetic coordinates .

| Station(Country) | Station Code | Geographic coordinates | | Geomagnetic coordinates | | LT (Hr) |
|---|---|---|---|---|---|---|
| Mtandika (Tanzania) | MTDK | 7.54 °S | 36.42 °E | 17.56 °S | 107.79 °E | UT+2:25 |
| Lusake (Zambia) | ZAMB | 15.43 °S | 28.31 °E | 16.93 °S | 77.96 °E | UT+2:00 |
| Malindi (Kenya) | MAL2 | 3.00 °S | 40.19 °E | 6.41 °S | 111.92 °E | UT+2:40 |
| Eldoret (Kenya) | MOIU | 0.28 °N | 35.29 °E | 2.68 °S | 107.72 °E | UT+2:20 |
| Addis-Ababa (Ethiopia) | ADIS | 9.04 °N | 38.77 °E | 5.35 °N | 112.53 °E | UT+2:35 |
| Solar village (Saudi Arabia) | SOLA | 24.26 °N | 46.51 °E | 17.71 °N | 118.16 °E | UT+3:00 |
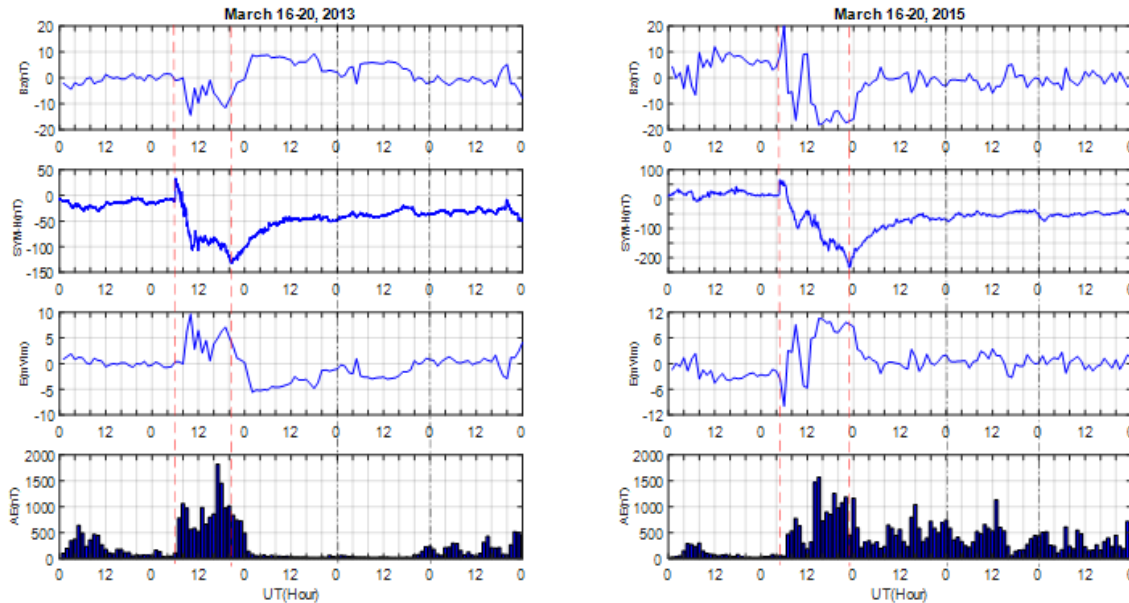


Figure 2. Some interplanetary and geomagnetic parameters between 16 and 20 March in year 2013 (left); and year 2015 (right).

storm's geo-effectiveness) and fluctuates till until it reached another peak ($\sim 18\ nT$) around 1400 UT on 17 March). The magnitude of IMF-Bz in the southward orientation remained substantial until around 2300 UT before decreasing to zero around 0500 UT. The shock occurred around 0500 UT on 17 March and produced a SYM-H value of $\sim 55\ nT$. The continuous injection of energy into the magnetosphere after the shock led to increase in the ring current and causing a depression in the SYM-H to a minimum of $-232\ nT$ around 2300 UT on 17 March. The interplanetary electric field, $E$ decreases abruptly around 0500 UT and then increases to a peak of $\sim 9\ mV/m$ around 0800 UT on 17 March. It then decreases again to a minimum value of $\sim 5.7\ mV/m$ (at 1100 UT) before increasing again to a peak ($\sim 10.6\ mV/m$) at 1400 UT and remained relatively constant till around 2300 UT before returning back to the pre-storm level few hours into the recovery phase. The AE-index increased to $\sim 780\ nT$ around 0800 UT on 17 March, decreases and then increases to a peak ($\sim 1600\ nT$) at 1400 UT on 17 March. AE-index remained relatively high for another 9 *hours* (i.e. until around 2300 UT).

### 3.2. Observations in 2013

During the March 2013 storm, as presented in Figure 3, the main phase (MP) of the storm showed daytime changes that are more prominent at stations north of the magnetic equator

(SOLA and ADIS). The post-sunset/pre-midnight peak in TEC during the MP is clearly formed only around the EIA trough station of MOIU and its southern station of MAL2, coinciding with the period of minimum SYM-H. Figure 3 could not capture distinct events at the beginning of the recovery phase (2000 UT or $\sim 2230 LT$), probably due to the low nighttime TEC magnitudes. However, with the aid of the quantifier presented in equation 1, Figure 4 reveals large enhancement from the beginning of the recovery phase (around 2000 UT on 17 March) and persisted for more than 7 *hours*, particularly at SOLA. There were other episodes of persistent depletions and some enhancement, but with smaller magnitude during the other recovery days at SOLA as well as some episodes of depletions (particularly at midnight) at the southern EIA crest regions (such as ZAMB). Generally, there seems to be consistent pattern of pre-midnight depletions at the EIA crest in both hemispheres during the recovery days.

For a clearer picture of events around seen in Figures 3 and 4, the line plots presented in Figure 5 showed the changes between the quiet and disturbed TEC along the latitudes in each hour. Though, the storm sudden commencement (SC) is around 0600 UT ($\sim 0830\ LT$), followed by immediate injection of ring current, deviation from quiet-time values (enhancements) started becoming visible around 0800 UT ($\sim 1030\ LT$), partic-
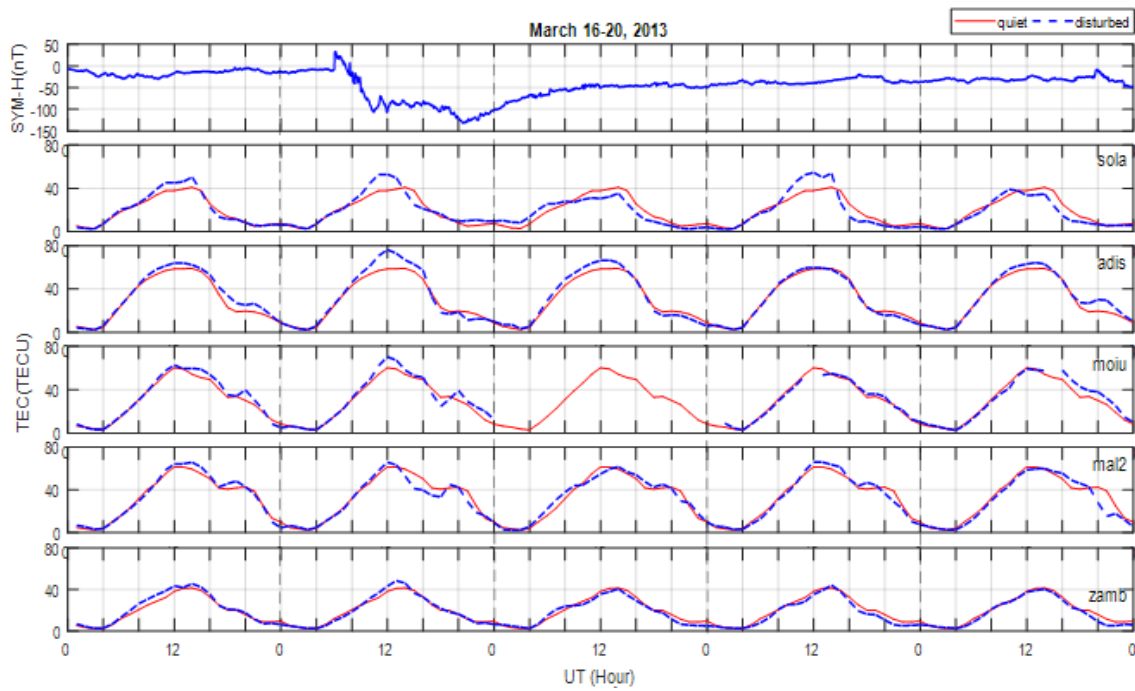
Figure 3. The superposed plot of quiet-time reference TEC (red solid curve) and the observed TEC (blue broken curve) during March 16 – 20, 2013 geomagnetic disturbance (The first panel shows the varying SYM-H index during the storm).
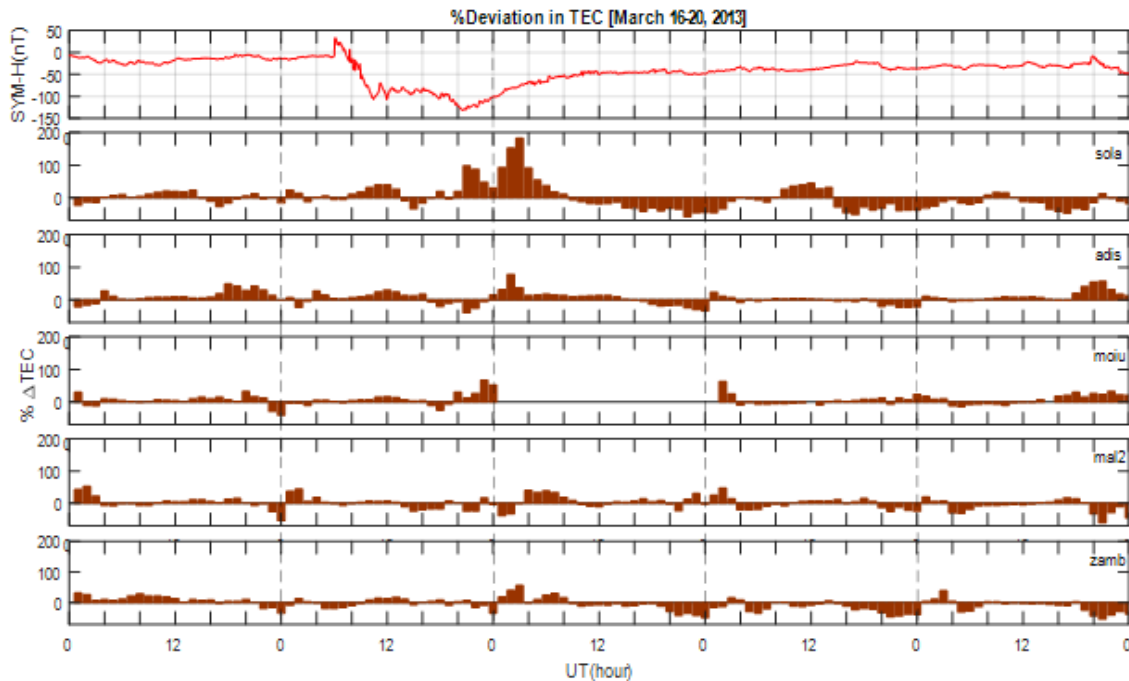


Figure 4. The percentage change in disturbed TEC with respect to the quiet-time reference value for the March 16 – 20, 2013 storm.

ularly in the north of the magnetic equator. The enhancements then extend to the EIA trough about an hour later (0900 UT or ~ 1130 $LT$). By 1000 UT (~ 1230 $LT$), the well-known day-time EIA trough of TEC magnitude had disappeared. Instead of a minimum TEC value at the trough flanked by two peak values on its either sides, there was a peak value higher than that of the southern EIA station. By 1300 UT (~ 1530 $LT$), depletions were beginning to set-in at the southern station and persisted till around 1700 UT. There was no substantial effect until 2000 UT (~ 2230 $LT$) where depletions towards the north and south crests. By 2200 UT (~ 0030 $LT$), the time around which the maximum SYM-H depression was observed, a prominent peak compared to the quiet-time value has been formed at the magnetic equator.
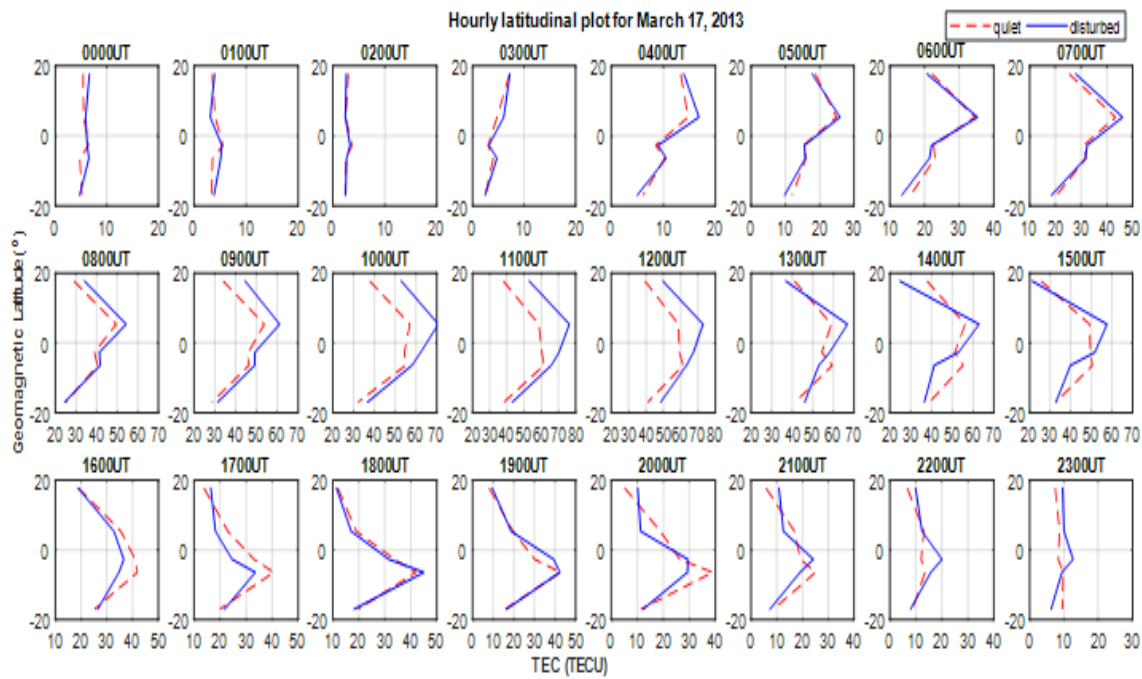
Figure 5. Latitudinal plot of quiet-time TEC (red broken curve) and the disturbed TEC (blue solid curve) for each hour during the 2013 storm day (17 March).
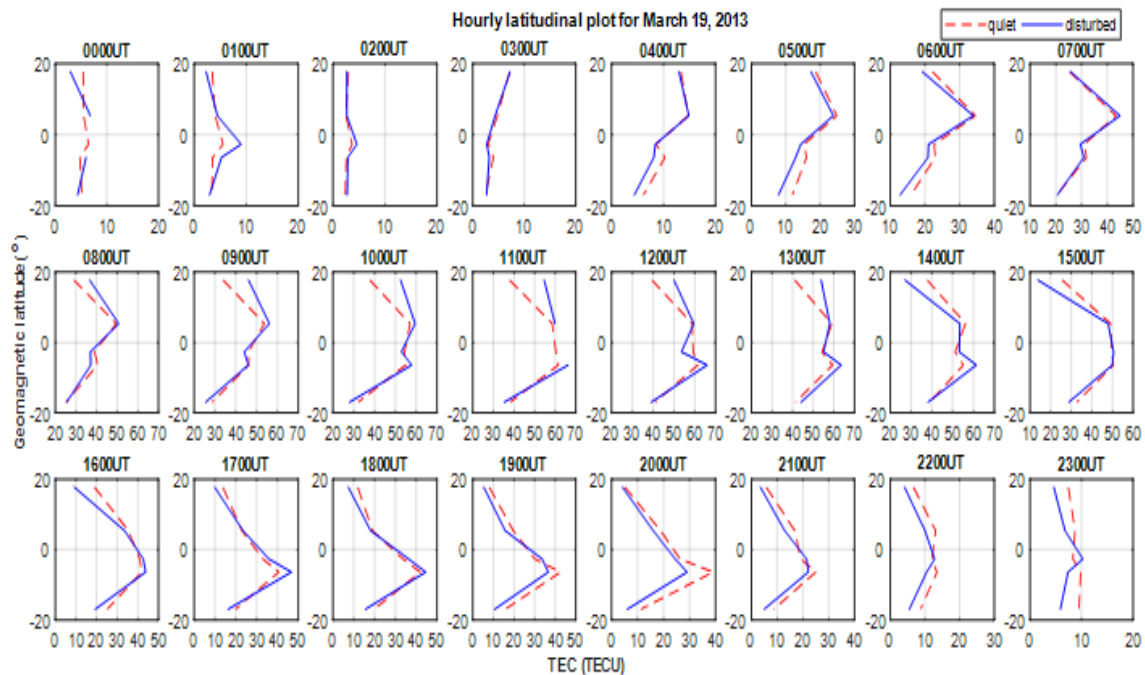
Figure 6. Same as Figure 5, but for 19 March 2013.

The recovery phase started just before 2300 UT on 17 March. However, the lack of data at MOIU on 18 March could not allow a detail analysis of the latitudinal variation of disturbed TEC with respect to the quiet-time values. On 19 March (Figure 6), the effect of the recovery phase was seen as slight TEC increase at the northern EIA station and decrease at the trough beginning from around 0900 UT (~ 1130 LT). This persisted till 1200 UT (~ 0230 UT) resulting in a stronger EIA during the storm than during quiet time. Also, from 2200 and 2300 UT, there was a total disappearance of the EIA structure compared to the quiet time morphology. The effect of the recovery phase on the EIA structure was also seen on 20 March (Figure 7), marked by slight TEC increase at the northern EIA station and decrease at the trough beginning from around 0800 UT (~ 1030

LT) and persisted till around 1100 UT (~ 0130 UT) resulting in a stronger EIA during the storm than during quiet time. Shortly after, decreases at the north most EIA station accompanied by increases at the EIA trough station was seen resulting into disappearance of the EIA at 1600 UT (~ 1830 LT). From 1900 (~ 2100 LT) – 2300 UT (~ 0100 LT), there was increase north of the equator and decreases at the south, indicating plasma movement from the south to the north without a change in the EIA structure from that of the quiet time.

### 3.3. Observations in 2015

During the March 2015 storm, as presented in Figure 8, the main phase (MP) of the storm showed changes that are more prominent towards the end of the main phase (1600 UT – 2300 UT) and for a larger part of the recovery phases at all stations. The post-sunset/pre-midnight peak in TEC during the main phase is clearly formed within the EIA region. Figure 9 reveals large changes between 1600 UT (~ 1830 LT) and 2300 UT (~ 0130 LT) with enhancement at the northern station of SOLA, which decreases towards the equator; then followed immediately by depletions at the equator and extended to the southern stations (MAL2 and MTDK). However, unlike the 2013 storm, deviations from quiet-time values due to the storm (enhancements) were not observed until around 1700 UT (~ 1930 LT), particularly in the north of the magnetic equator and the EIA trough station. The deviations (depletions) then extend to stations south of the magnetic equator about four hours later (2100 UT or ~ 2330 LT). The depletions at the southern stations coincided with the beginning of the recovery phase. The first day of the recovery phase (18 March) is characterized by consistent enhancements at all stations between 0300 UT (~ 0530 LT) and 0700 UT (~ 0930 LT), brief episode of depletions around 1400 UT (~ 1630 LT) and longer episode of depletions which extends till the next recovery day (19 March) (2000 UT – 0300 UT) at the southern stations. The depletions lasted more than 12 hours at MTDK with larger amplitudes around 2300 UT (~ 0130 LT). On other recovery days (19 and 20 March), there were other episodes of enhancements at ADIS between 1800 UT (~ 2030 LT) and 2300 UT (~ 0130 LT) (as well as 18 March) and depletions, but with smaller magnitude, during the other recovery days at SOLA as well as the southern EIA crest regions (such as ZAMB). These depletions were persistent occurring for the larger part of the days. Generally, there seems to be consistent pattern of pre-midnight depletions at the EIA crest in both hemispheres during the recovery days, except at ADIS.

For a clearer picture of events around seen in Figures 8 and 9, the line plots presented in Figures 10 – 14 showed the changes between the quiet and disturbed TEC along the latitudes in each hour. First for the storm day (17 March), the storm SC is around 0500 UT (~ 0730 LT), around same period as that of the 2013 event, followed by immediate injection of ring current. There was no modification of the EIA structure, but slight deviations in form of depletions at all stations become visible at the instance of the SC until 0700 UT (~ 0930 LT) and between 1100 and 1400 UT (~ 1330 and 1630 LT) although, these deviations cannot be regarded as storm-induced since the $|\%\Delta TEC|$

is less than 25 (see Figure 9). However, beginning from around 1600 UT (~ 1830 LT), there was substantial modification of the EIA; there was rapid enhancement at the northern EIA crest stations. These led to a reversal of the most prominent peaks. While the peak in the southern hemisphere is greater than that of the north during quiet period, the storm reversed this and caused the peak in the northern hemisphere to be greater. This persisted until 2300 UT (~ 0130 LT on 18 March). However, there was decrease in the magnitude of the enhancements at the northern stations simultaneously with depletions at the southern stations.

On the first day of the recovery phase (18 March), the modification of the EIA structure continued with the disappearance of the quiet-time peak at the equator between 0100 and 0200 UT (~ 0330 and 0430 LT). There were enhancements beginning from 0400 UT (~ 0630 LT) at all stations and lasted till around 0800 UT (~ 1030 LT) accompanied by a more prominent peak at the southern crest region. The enhancement persisted until 1000 UT (~ 1230 LT) at the equator, leading to the disappearance of the equatorial trough. The immediate accompanying depletions at the southern stations led to the formation of only one peak (i.e. the northern peak) at 1100 UT (~ 1330 LT). However, the depletions in the south continued, but with decreased magnitude, until another peak is formed at the equator around 1600 UT (~ 1830 LT). Then enhancements in the north of the equator beginning from 1700 UT (~ 1930 LT) led to the formation of only one peak (i.e. the northern peak) due to the disappearance of the southern peak. This persisted until 2300 UT. Observations during the other recovery days (19 and 20 March) (Figures 12 and 13) are similar to observations on the first day.

## 4. Discussion

Electric field action with the perpendicular northward horizontal component of the Earth's magnetic field around the magnetic equator plays a very important role in plasma movement along the equatorial latitudes. This action accounts for changes in the daytime equatorial morphology of the ionospheric electron density during quiet time. The daytime eastward orientation of the electric field causes upward motion of the plasma to higher altitudes (region of lower recombination rates) over the equator, and then the plasma diffuses along magnetic lines to either sides of the equator. This leads to a trough of plasma density at the equator and two crests at either side. At nighttime, when the orientation of the electric field is westward, plasma moves back to lower altitudes. This may lead to collapse of the EIA structure, but this is not the case, as the plasma fountain effect is sustained by slow decay rate of the F-layer plasma during recombination [22, 23]. The PRE and/or the slow F-layer plasma decay rate, both occurring in the absence of strong solar control, inhibit plasma movement from the EIA crests to the trough [24, 25, 26].

During disturbed time, the ejection of disturbed electric fields (both the PPEF and DDEF), modifies plasma distribution depending on the local time. For example, Tsurutani *et al.* [22] attributed increase in EIA intensity to the unusual increase in
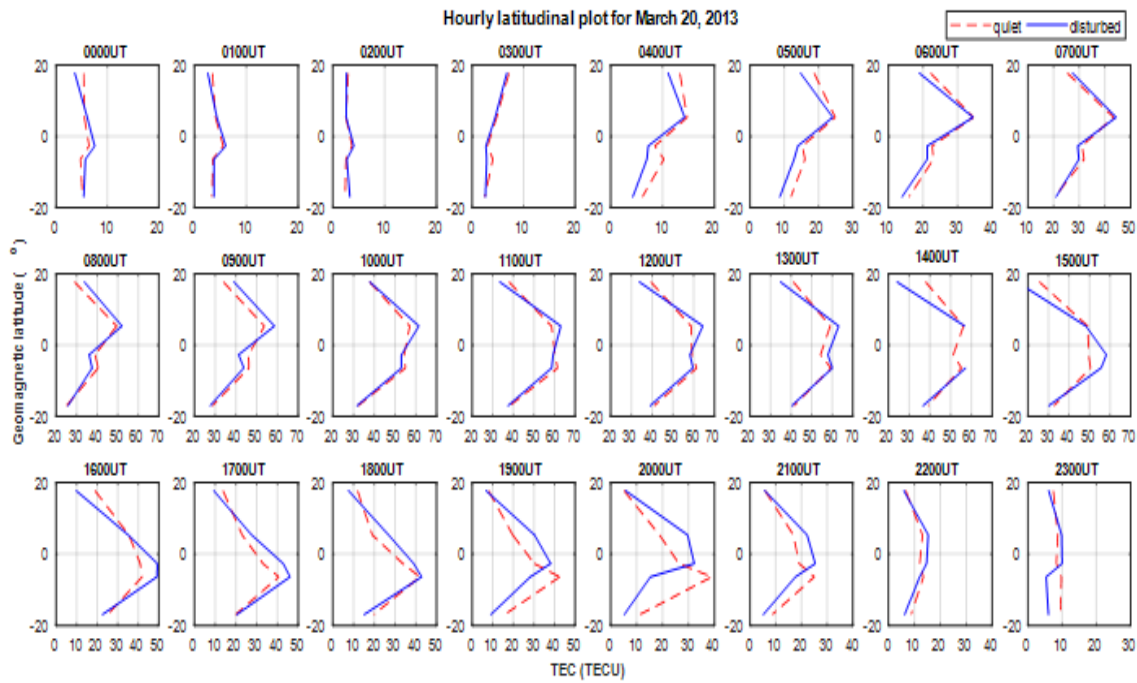
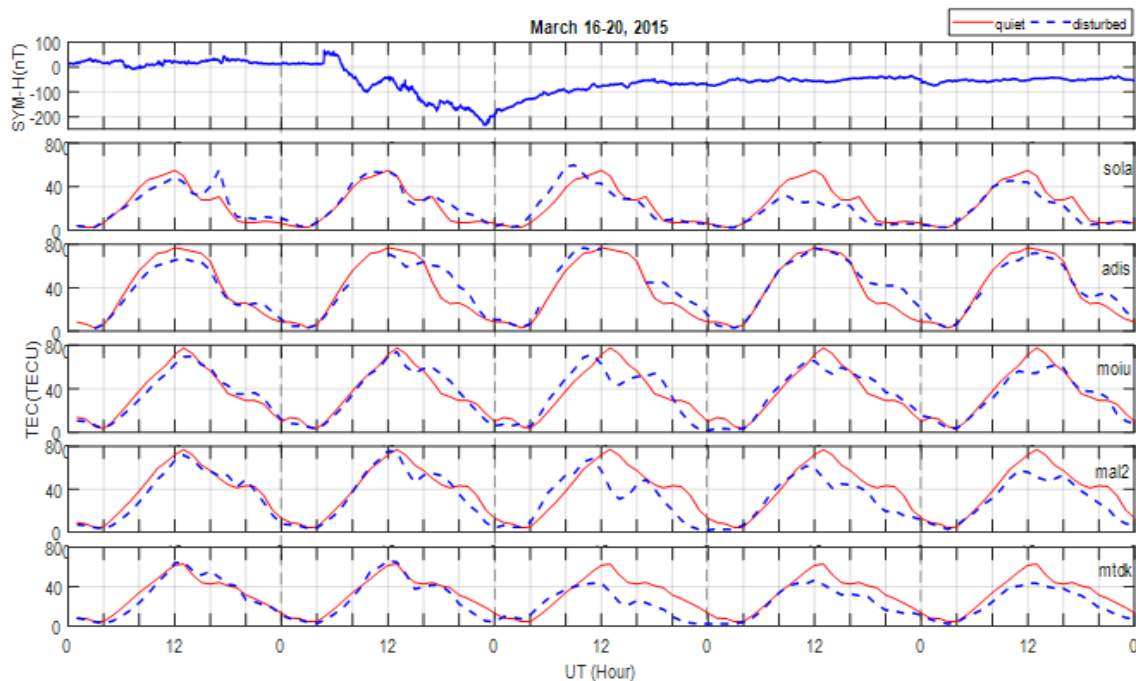Figure 7. Same as Figure 5, but for 20 March 2013.



Figure 8. The superposed plot of quiet-time reference TEC (red solid curve) and the observed TEC (blue broken curve) during March 16 − 20, 2015 geomagnetic disturbance (The first panel shows the varying SYM-H index during the storm).

the eastward electric field due to PPEF. The PPEF causes lifting of the ionospheric plasma to unusual altitudes, and the diffused plasma now concentrates at latitudes farther away from the magnetic equator. Hence, the EIA crests during the disturbance form at latitudes higher than those of the quiet periods while the ongoing/concurrent ionization at lower heights continue to produce plasma that replenish the trough. As a result,

the EIA structure is maintained, but with the crests at higher latitudes and TEC magnitude increasing across all latitudes in the EIA region.Increase in the F-region electric field during pre-reversal enhancement (PRE) can also maintain or increase the strength of the plasma fountain effect [27, 28]. The DDEF, a delayed modification of the electric field acting to suppress the solar quiet (Sq) electric field, usually accounts for plasma dis-
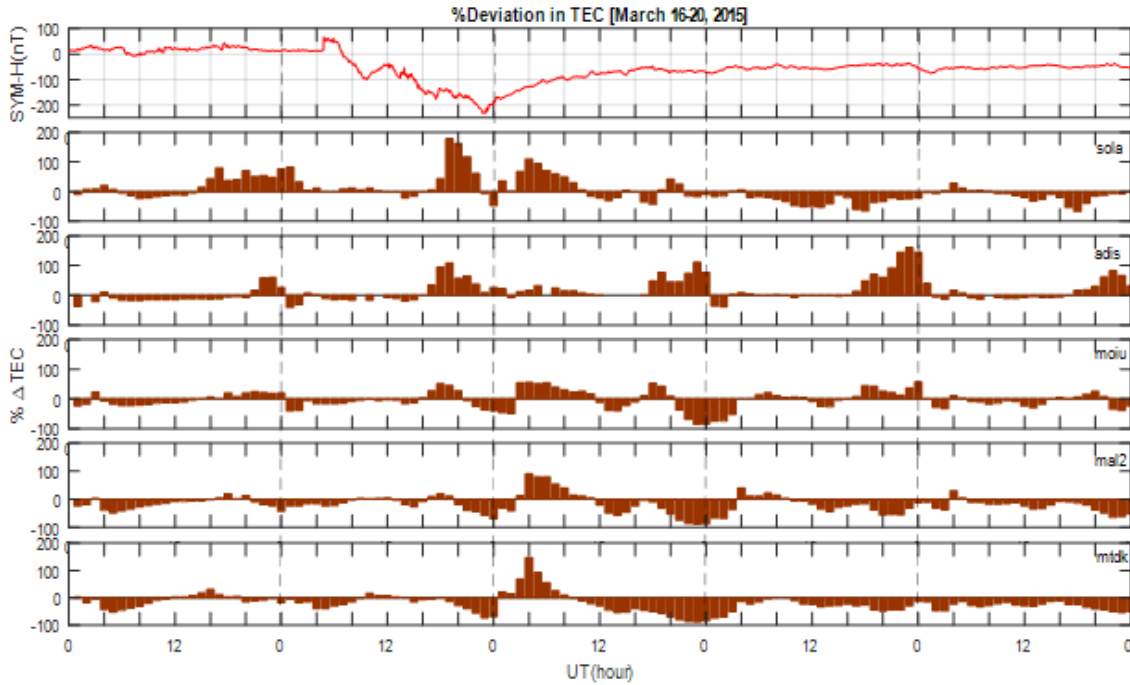
Figure 9. The percentage change in disturbed TEC with respect to the quiet-time reference value for the March 16 – 20, 2015 storm.
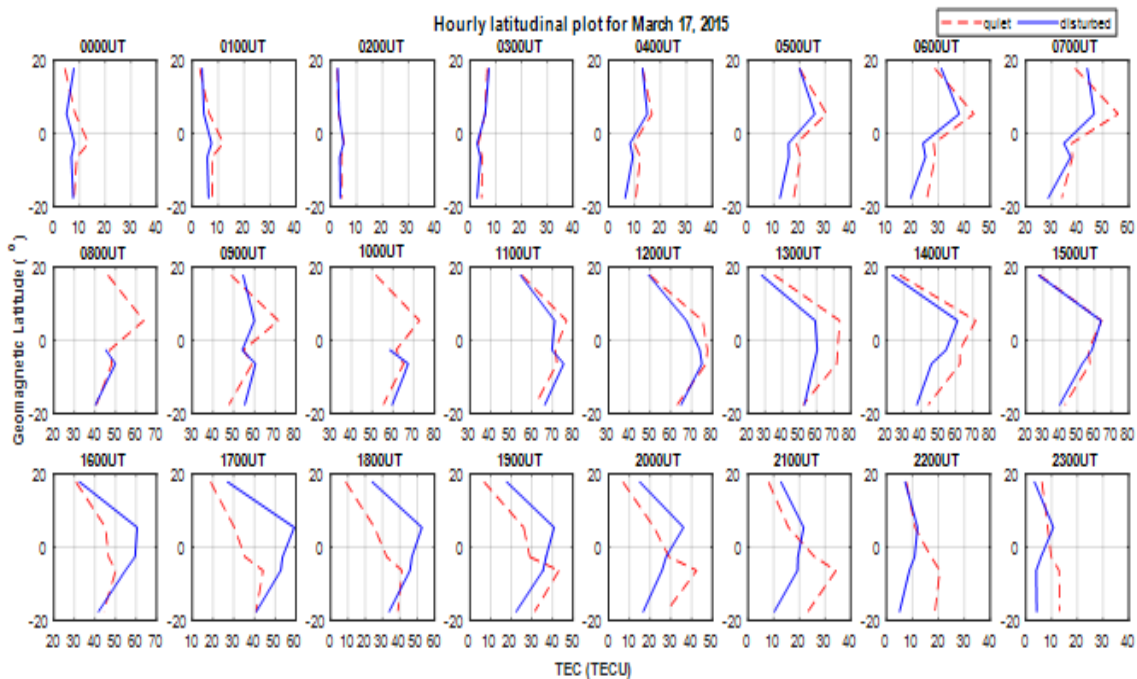


Figure 10. Latitudinal plot of quiet-time TEC (red broken curve) and the disturbed TEC (blue solid curve) for each hour during the 2015 storm day (17 March).

tribution to leads to changes in the EIA structure depending on the local time. Thus, DDEF causes eastward electric field to be westward, thereby weakening the EIA structure or causing its totally disappearance and vice-versa. Another modification factor to plasma during storm events, particularly the prolonged positive/negative storm effects irrespective of local time is the thermospheric circulation. Mendillo [29] noted that changes to

$O/N_2$ composition ratio such as increase/decrease in the ratio may drive positive/negative phases respectively.

The more prominent in enhancements, particularly at stations north of the equator (SOLA and ADIS) during the March 2013 storm's MP and the post-sunset/pre-midnight peak in TEC towards the end of the MP (as observed from Figure 3) signals the to the action of the PPEF. The large enhancement from
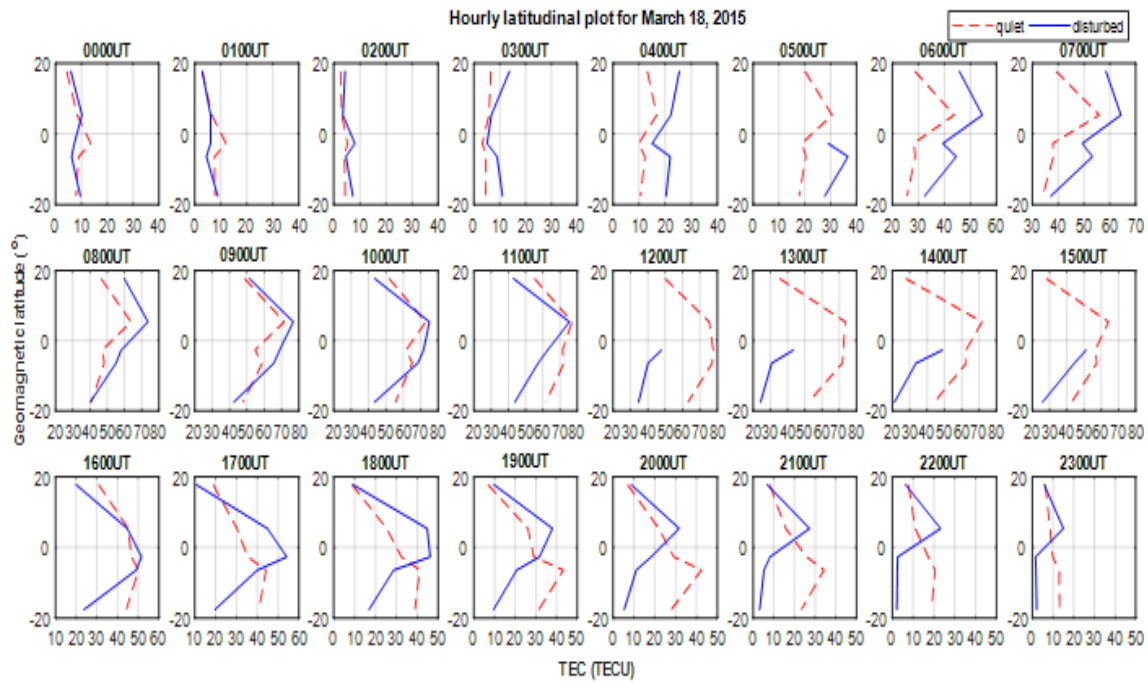
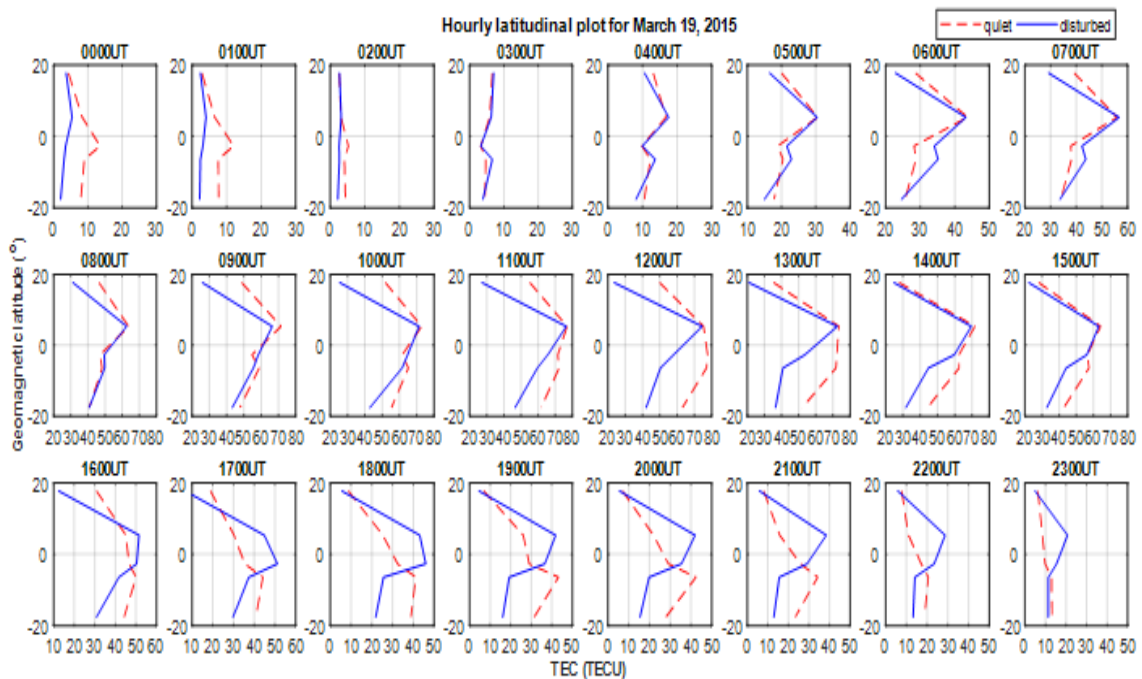Figure 11. Same as Figure 10, but for 18 March 2015.



Figure 12. Same as Figure 10, but for 19 March 2015.

the beginning of the recovery phase in the northern and persisted for more than 7 hours, particularly at SOLA (as seen from Figure 4) may be due to the nighttime eastward electric field caused by the DDEF. This leads to plasma movement to the low latitudes (i.e. the EIA crest) from the equator. The other episodes of depletions during the remaining recovery period are prolonged suggesting the role of changing thermospheric composition. This resonates with [12] who attributed the negative

phases observed in the Asian sector during the 2013 event to electric field dynamics and changing thermospheric composition. Observations from Figures 5 – 7 provide hourly consideration of plasma-redistribution during the entire 2013 storm event. The asymmetry in enhancements on either side of the equator between 0800 and 1200 UT (~ 1030 and ~ 1430 LT) and followed by the disappearance of the EIA structure between 1000 and 1200 UT (~ 1230 and ~ 1430 LT) may be due to
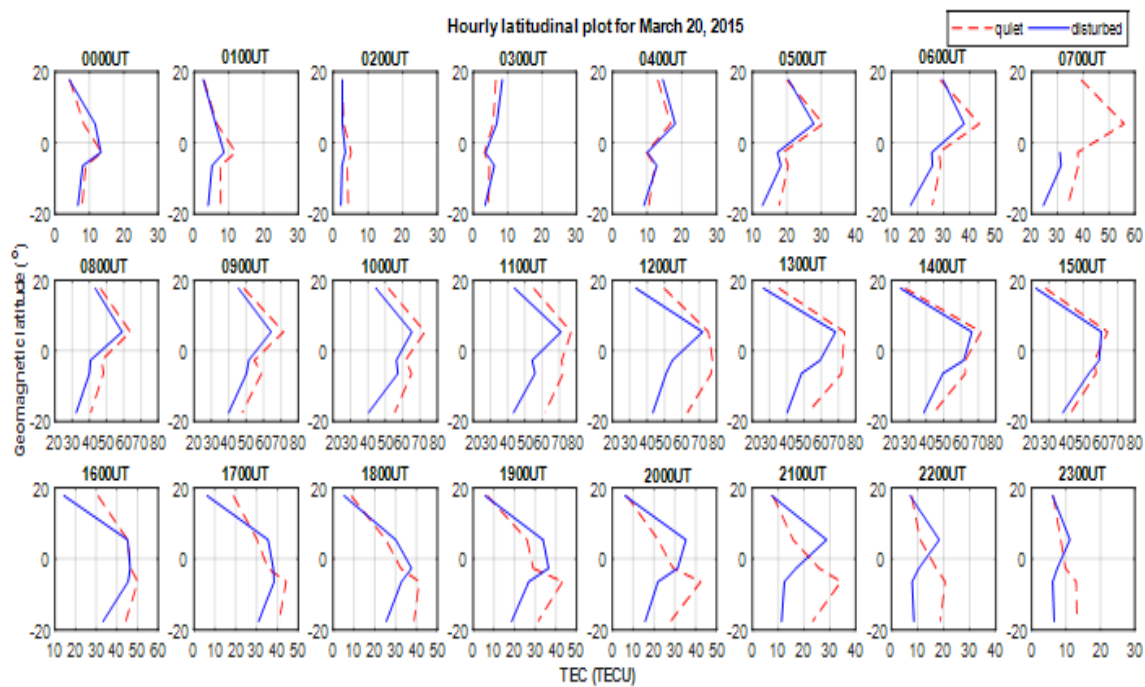
Figure 13. Same as Figure 10, but for 20 March 2015.

plasma injection from higher latitudes in the northern region. If it were to be due to PPEF, it is expected that the EIA will be strengthened. However, this was not so, rather, a large increase in the north and a higher magnitude at the trough than the south was observed. For four stations in the south of the EIA as documented by [4], there were little or no TEC changes during the MP. Apart from the continued disappearance of the EIA structure, the peak at the north of the EIA persisted and accompanied by reduction in TEC magnitude at either side of the equator between 1300 and 1500 UT (~ 1530 and ~ 1730 LT). This may be explained in terms of reduction in ionization and plasma drifting towards the EIA trough. Therefore, by 1600 UT (~ 1830 LT), the EIA has returned to its quiet-time structure.

At the beginning of the recovery phase (2100 UT / ~ 2330 LT), the appearance of a peak TEC value at the EIA trough (deviation from the quiet-time EIA structure) was seen an it persisted for about 3 hours. This is due to the DDEF which is known to suppress quiet-time EIA structure. The other modifications of the EIA structure during the 2013 event are on 19 March around 1200 UT (where the structure is strengthened) and 2200 – 2300 UT (where the structure is slightly suppressed) as well as 20 March around 0300 – 0600 UT, 1500 UT and 2200 – 2300 UT (where the structure is suppressed). The short duration of these observations may not be attributable to the storm or could be due to the nature of the storm, where the processes such as the impact of the DDEF is short-lived. For example, DDEF around 1200 UT (~ 1430 LT) on 19 March is expected to decrease the influence of the eastward electric field. However, substantial storm-induced changes are expected to persist for more than two hours. Therefore, the limitations of observational equipment could not allow for further investigation to identify the mechanism involved.

During the 2015 event, prominent observations are towards the end of the main phase (1600 UT – 2300 UT) and for a larger part of the recovery phases at all stations. This is a clear deviation from report by [12] and [30], where a short-lived enhancement was observed around 1200 UT at the Asian sector (~ 1900 LT). The prominent post-sunset/pre-midnight peak in TEC during the main phase at all the stations with higher magnitude than the quiet-time value within the EIA may be due to PPEF. The enhancements between 1600 UT (~ 1830 LT) on 17 March and 2300 UT (~ 0130 LT on 18 March) north of the equator, then followed immediately by depletions at the equator and extended to the southern stations on the storm day could be as a result of movement of plasma from higher latitudes in the north across the equator to the south. The absence of daytime enhancements/depletions particularly during the MP may be due to the result of the overlapping actions of PPEF and DDEF. According to Hairston *et al.* [6], the DDEF dominates the PPEF for a larger period of MP. The depletions at the southern stations occurring around the beginning of the recovery phase could be attributed to the DDEF. However, its interaction with the PPEF limits the magnitude of the depletions. Ikubanni *et al.* [4] also reported a 5-hour duration of depletion-sat the southern EIA stations around the period of minimum SYM-H. Recall that the [19] had shown that the EIA crests in the African sector formed beyond $15^o$ N and in the south just below geographical equator. Thus, the EIA trough is expected to form midway, where ADIS is located. Hence, the persistent and long-lasting evening/nighttime depletions at stations other than ADIS, where enhancements were observed, the on all the recovery days could be due to the role of the changing $O/N_2$ ratio. Increase in $O$ around the EIA trough region leads to enhancement while increase in $N_2$ at higher latitudes causes

depletions.

## 5. Conclusion

With data from stations along the eastern corridor of the African sector, taking account the local time differences, we have studied the movement of plasma across the stations. Clear distinctions in the responses to the events both during the MP and the recovery phase were observed. The most prominent effect of the 2013 storm was at the beginning of the recovery phase particularly at the EIA crest station of SOLA. For the 2015 event, substantial effects were observed towards the end of the MP as well as throughout the entire recovery phase, extending into hours. The dynamical roles of several factors were discussed in line with the observations.The study of the two storms showed that recovery phases may experience larger amplitudes of depletions/enhancements than the main phase depending on the magnitude of the event and other accompanying processes. Improved instrumentation in Africa will aid in better investigation of future space weather events on the African geospacer.

## Acknowledgments

## References

[1] Z. Xu, M. D. Hartinger, C.R. Clauer, T. Peek, R. Behlke, "A comparison of the ground magnetic responses during the 2013 and 2015 St. Patrick's Day geomagnetic storms", J. Geophys. Res. Space Physics, **122** (2017) 036, doi:10.1002/2016JA023338.

[2] B. O. Adebesin , "Roles of interplanetary and geomagnetic parameters in intense and very intense magnetic storms generation and their geoeffectiveness", Acta Geod. Geoph. Hung., **43**(2008) 383, doi:10.1556/AGeod.43.2008.4.2.

[3] K. S. Jacobsen & Y. L. Andalsvik, "Overview of the 2015 St. Patrick's day storm and its consequences for RTK and PPP positioning in Norway", J. Space Weather Space Clim., **6**(2016) A9, doi:10.1051/swsc/2016004.

[4] S. O. Ikubanni, S. J. Adebiyi, B. O. Adebesin, K. O. Dopamu, B. W. Joshua, O. S. Bolaji & B. J. Adekoya, "Response of GPS-TEC in the African Equatorial Region to the Two Recent St. Patrick's Day Storms", International Journal of Civil Engineering and Technology, **9**(2018) 773.

[5] S. -R. Zhang, Y. Zhang, W. Wang & O. P Verkhoglyadova, "Geospace system responses to the St. Patrick's Day storms in 2013 and 2015", J. Geophys. Res. Space Physics, **122**(2017), doi:10.1002/2017JA024232.

[6] M. Hairston, W. R. Coley & R. Stoneback, "Responses in the polar and equatorial ionosphere to the March 2015 St. Patrick Day storm, J. Geophys. Res. Space Physics, **121**(2016) 213, doi:10.1002/2016JA023165.

[7] S. Basu, BasuSu., K. M. Groves, E. MacKenzie, M. J. Keskinen & F. J. Rich, "Near-simultaneous plasma structuring in the midlatitude and equatorial ionosphere during magnetic superstorms", Geophy. Res. Lett., **32**(2005) L12S05, doi:10.1029/2004GL021678.

[8] Y. Wei, B. Zhao, G. Li & W. Wan, "Electric field penetration into Earth's ionosphere: A brief review for 2000–2013", Sci. Bull., **60**(2015) 748, doi:10.1007/s11434-015-0749-4.

[9] J. Kuai, L. Liu,J. Liu, S. Sripathi, B. Zhao, Y. Chen, H. Le & L. Hu, "Effects of disturbed electric fields in the low-latitude and equatorial ionosphere during the 2015 St. Patrick's Day storm",J. Geophys. Res. Space Physics, **121**(2016), doi:10.1002/2016JA022832.

[10] Ramsingh, S. Sripathi, S. Sreekumar, S. Banola, K. Emperumal, P. Tiwari & B. S. Kumar, "Low-latitude ionosphere response to supergeomagnetic storm of 17/18 March 2015: Results from a chain of ground-based observations over Indian sector", J. Geophys. Res. Space Physics, **120**(2015) 864, doi:10.1002/2015JA021509.

[11] Tulasi Ram, T. Yokoyama, Y. Otsuka, K. Shiokawa, S. Sripathi, B. Veenadhari, R. Heelis, K. K. Ajith, V. S. Gowtam, S. Gurubaran, P. Supnithi & M. L. Huy, "Duskside enhancement of equatorial zonal electric field response to convection electric fields during the St.Patrick's Day storm on 17 March 2015", J. Geophys. Res. Space Physics, **121**(2016) 538, doi:10.1002/2015JA021932.

[12] B. R. Kalita, R. Hazarika, G. Kakoti, P. K. Bhuyan, D. Chakrabarty, G. K. Seemala, K. Wang, S. Sharma, T. Yokoyama, P. Supnithi, T. Komolmis, C. Y. Yatimi, M. L. Huy & P. Roy, "Conjugate hemisphere ionospheric response to the St. Patrick's Day storms of 2013 and 2015 in the 100oE longitudinal sector", J. Geophys. Res. Space Physics, **121**(2016) 11364, https://doi.org/10.1002/2016JA023119.

[13] B. Nava, J. Rodriguez-Zuluaga, K. Alazo-Cuartas, A. Kashchyev, Y. Migoya-Orue, S. M. Radicella, C. Amory-Mazaudier & R. Fleury, "Middle and low latitude ionosphere response to 2015 St. Patrick's Day geomagnetic storm", J. Geophys. Res. Space Physics, (2016), doi:10.1002/2015JA022299.

[14] C. -S.Huang, G. R. Wilson, M. R. Hairston, Y. Zhang, W. Wang & J. Liu, "Equatorial ionospheric plasma drifts and O+ concentration enhancements associated with disturbance dynamo during the 2015 St. Patrick's Daymagnetic storm", J. Geophys. Res. Space Physics, **121**(2016) 961, doi:10.1002/2016JA023072.

[15] W. Luo, Z. Zhu & J. Lan, "The strength and hemispheric asymmetry of Equatorial Ionization Anomaly during two geomagnetic storms in 2013 from Global Ionosphere Map and SAMI2", J. Atmos. Sol.-Terr. Phys., **146**(2016) 101, doi:10.1016/j.jastp.2016.05.012.

[16] J. Zhong, W. Wang, X. Yue, A. G. Burns, X. Dou & J. Lei, "Long-duration depletion in the topside ionospheric total electron content during the recovery phase of the March 2015 strong storm", J. Geophys. Res. Space Physics, **121**(2016) 4733, doi:10.1002/2016JA022469.

[17] C. Borries, A. M. Mahrous, N. M. Ellahouny & R. Badeke, "Multiple ionospheric perturbations during the Saint Patrick's Day storm 2015 in the European-African sector", J. Geophys. Res. Space Physics, **121**(2016) 333, https://doi.org/10.1002/2016JA023178.

[18] J. B. Habarulema, E. Yizengaw, Z. T. Katamzi-Joseph, M. B. Moldwin & S. Buchert, "Storm time global observations of large-scale TIDs from ground-based and in-situ satellite measurements", J. Geophys. Res. Space Physics, **123**(2017) 711, https://doi.org/10.1002/2017JA024510.

[19] P. O. Amaechi, E. O. Oyeyemi & A. O. Akala, "Geomagnetic storm effects on the occurrences of ionospheric irregularities over the African equatorial/low-latitude region", Advances in Space Research, **61**(2018) 2070.

[20] O. S. Bolaji, S. J. Adebiyi & J. B. Fashae, "Characterization of ionospheric irregularities at different longitudes during quiet and disturbed geomagnetic conditions", J. Atmos. Solar Terr. Physics, **182**(2019) 93, https://doi.org/10.1016/j.jastp.2018.11.007.

[21] J. A. Wanliss & K. M. Showalter, "High-resolution global storm index: Dst versus SYM-H", J. Geophys. Res., **111**(2006) A02202, doi:10.1029/2005JA01103.

[22] B. T. Tsurutani, A. Mannucci, B. Lijima, M. A. Abdu, J. H. A. Sobral, W. Gonzalez, F. Guarnieri, T. Tsuda, A. Saito, K. Yumoto, B. Fejer, T. J. Fuller-Rowell, J. Kozyra, J. C. Foster, A. Coster & V. M. Vasyliunas, "Global dayside ionospheric uplift and enhancement associated with interplanetary electric fields", J. Geophys. Res. Space Physics, **109**(2004), https://doi.org/10.1002/2003JA010342.

[23] B. T. Tsurutani, O. P. Verkhoglyadova, A. J. Mannucci, A. Saito, T. Araki, K. Yumoto, T. Tsuda, M. A. Abdu, J. H. A. Sobral, W. D. Gonzalez, H. McCreadie, G. S. Lakhina & V. M. Vasyliunas, "Prompt penetration electric field (PPEFs) and their ionospheric origin during the great mag-

netic storm of 30-31 October 2003", J. Geophys. Res. Space Physics, **113**(2008), A05311,https://doi.org/10.1029/2007JA012879.

[24] N. Balan & G. J. Bailey, "Equatorial plasma fountain and its effects: Possibility of an additional layer", J. Geophys. Res. Space Physics, **100**(1995) 21421.

[25] N. Balan, G. J. Bailey, K. I. Oyama, P. G. Richards, J. MacBougall & I. S. Batista, "Equatorial plasma fountain and its effects over three locations: Evidence for an additional layer, the F3 layer", J. Geophys. Res. Space Physics, **102**(1997) 2047.

[26] G. J. Bailey, N. Balan & Y. Z. Su, "The Sheffield University ionosphere plasma sphere model - a review", J. Atmos. Terr. Phys., **59**(1997) 1541.

[27] D. J. Crain, J. J. Sojka, R. W. Schunk & L. Zhu, "Parameterized study of the ionospheric modification associated with sun-aligned polar cap arcs",

J. Geophys. Res. **98**(1993) 6151.

[28] R. A. Heelis, "Electrodynamics in the low and middle latitude ionosphere: A tutorial", J. Atmos. Sol. Terr. Physics, **66**(2004) 825.

[29] M. Mendillo, "Storms in the ionosphere: patterns and processes for total electron content", Rev. Geophys., **44**(2006) RG4001, doi:10.1029/2005RG000193.

[30] C. Jiang, G. Yang, J. Liu, T. Yokoyama, T. Liu, T. Lan, C. Zhou, Y. Zhang, Z. Zhao, T. Komolmis, P. Supnithi & C. Y. Yatini, "Equatorial and low-latitude ionospheric response to the 17-18 March 2015 great storm over Southeast Asia longitude sector", J. Geophys. Res. Space Physics, **122**(2017), https://doi.org/10.1002/2017JA024134.